J. Fluid Mech. (1981), *vol.* 112, *pp.* 161–188
Printed in Great Britain

The rotating hydraulics of the open-channel flow between two basins

By COLIN Y. SHEN

Department of Oceanography, University of Washington,
Seattle, Washington 98195

(Received 17 September 1979 and in revised form 20 February 1981)

The theory of rotating open-channel flow between two basins is presented and experimentally verified for three cases. The first case considered is the submerged weir-flow, i.e. the height of the channel floor is below the free-surface height of the fluid in the lower basin. Flow for this case is found to depend on the fluid level in the downstream basin when the fluid level there is high and is independent of the fluid level downstream as soon as the level falls below a critical height; at that point the flow in the channel becomes critical (controlled). The dependence of the flow on upstream potential vorticity and on rotation rate is also examined. It is shown that transport of the flow decreases whenever rotation rate or upstream potential vorticity is increased. The second case studied is controlled flow through a channel of irregular cross section (the truncated channel). Transport of this flow is shown to increase at some moderate rotations if the channel floor has a cross-channel slope similar to that of the surface of the current. Otherwise, the transport always decreases with rotation rate. The final case is concerned with supercritical separation of the current downstream of the control section, i.e. the current separates from the left wall of the channel (looking downstream). Visual evidence and measurements of formation of such a boundary current are obtained. Comparisons between the theory and the experiment for the three cases are generally reasonable except when flow separates in the control section; the theory is found inapplicable to such separation.

1. Introduction

The classical hydraulics of flow over a weir (or dam) from a reservoir has been re-investigated in recent years for a rotating fluid system. Renewed interest in this classical problem is motivated by its possible use as a model for studying the flow of dense bottom water over submarine ridges. Such a model is feasible because observations (Stalcup, Metcalf & Johnson 1975; Lonsdale 1977; Worthington 1970) have shown that the submarine ridge often acts as a dam in trapping the bottom water and restricting flow of the water to narrow straits and shallow sills atop the ridge.

In the ocean the effect of the earth's rotation on the current is important, so it has been necessary to study weir flow in a rotating frame of reference. There have been several investigations of this rotating weir problem; Stern (1972, 1974) studied theoretically the stability of the flow at the weir section. Whitehead, Leetmaa & Knox (1974) and Sambuco & Whitehead (1976) presented both theory and experiments for zero potential vorticity flow over a weir, i.e. the flow coming from a deep

basin. Later, in a more detailed theoretical study, Gill (1977) obtained results for finite potential vorticity flows applicable to basins of all depths.

In this paper, additional theoretical and experimental investigation of the rotating weir flow will be presented. Specifically, three problems will be considered. The first one is constant potential vorticity flow over a submerged weir, in which sill height is below the free-surface level of the fluid in the downstream reservoir as opposed to the case in which the free surface is below the sill as investigated previously. The second one is controlled zero potential vorticity flow through a channel of irregular cross section (henceforth, the channel refers to that part of weir where the water overflows). This is a generalization of the problem studied by Whitehead *et al.* (1974). They previously studied the flow through a rectangular channel. The effect of an irregular channel geometry will be examined here. The third problem is concerned with supercritical separation of the current. The current will be shown to separate from the left channel wall in the downstream section of the weir (in this paper, left and right are for an observer looking downstream). Evidence of the formation of the boundary current will be obtained and the location of the separation will be examined. This problem is relevant to the ocean bottom boundary current observed downstream of sea straits (for example Worthington 1970).

Investigation of these three problems represents some extension and generalization of previous studies. Equally important, experimental verification of the theory will also represent a further test of the concept of hydraulic control. This concept is an essential element in the theoretical description of weir flows. Simply stated (see also § 2), it asserts that the flow speed should be equal to the long-wave speed at the narrowest section (called the control section) of the weir. The implication of this 'control' statement is that the current in the weir should be insensitive to downstream conditions since disturbance downstream cannot propagate past the control section. In non-rotating hydraulics, such control by the weir has been proved to be of considerable practical value in determining weir flow, since the problem is now greatly simplified with omission of the downstream condition, which is often difficult to specify and pose properly. (The theoretical basis of hydraulic control follows from consideration of the flow over a weir having a smooth and gradually varying downstream geometry. Gill (1977) has given a general theoretical demonstration of the control by the weir under this assumption of smooth geometry. In practice, the geometry for realization of the control is not so restrictive, as frequently demonstrated in non-rotating hydraulics.) Whether the same concept of hydraulic control is applicable to rotating open-channel flow under different downstream conditions is obviously of interest. The problems considered here will permit a test of the concept for rotating flow subjected to different downstream conditions. In the problem of submerged weir-flow, the downstream fluid level will be varied. In the problem of the irregular channel, the control section is non-uniform, and the downstream section of the weir has an abrupt end. Lastly in the problem of supercritical separation, the downstream section has a flared opening. The theoretical description of the problems, however, will proceed as usual under the assumption of a gradually varying channel.

This paper, therefore, will begin in § 2 with the governing equations for an open channel under this assumption and a discussion of the concept of hydraulic control. In § 3, a theoretical discussion of the three problems mentioned above will be presented. The experiments are then described in § 4. Theory and experiment are compared for

the three cases in § 5. The results are summarized and their relevance to the ocean currents in straits and sills are discussed in § 6.

2. Equations for rotating open channel flows

Essential to the description of channel flow is the approximation that the geometry of the channel varies slowly along the direction of the flow. This makes the problem tractable and yet still retains some nonlinearities of the flow through the conservation of the Bernoulli function and the potential vorticity. For the convenience of the subsequent discussion as well as to establish notation, we shall state the equations of motion under the approximation and some results concerning hydraulic control.

The approximation essentially comes in two stages. The first is that the vertical elevation of the channel floor varies gradually. In this case, vertical velocity and vertical acceleration are negligible and the equations reduce to the familiar shallow water equations (for a homogeneous fluid),

$$\mathbf{U}.\nabla_l \mathbf{U} + f\hat{\mathbf{k}} \times \mathbf{U} = -\nabla P, \tag{2.1a}$$

$$\partial P/\partial z = -g, \tag{2.1b}$$

$$\nabla_l . \mathbf{U}H = 0, \tag{2.1c}$$

where $\mathbf{U} = u\hat{\mathbf{i}} + v\hat{\mathbf{j}}$ is the horizontal velocity vector (see figure 1 (*a*) for the co-ordinate system), P the pressure divided by the density of the fluid, f twice the frequency of the rotation, g the gravity, H the thickness of the fluid, and $\nabla_l = (\partial/\partial x)\hat{\mathbf{i}} + (\partial/\partial y)\hat{\mathbf{j}}$.

The above equations can be manipulated to yield two equally familiar conservation equations which are the Bernoulli equation,

$$\mathbf{U}.\nabla_l [\tfrac{1}{2}|\mathbf{U}|^2 + g(H+\eta)] = 0, \tag{2.2}$$

where η is the elevation of the channel floor, and the potential vorticity equation,

$$\mathbf{U}.\nabla_l [(\hat{\mathbf{k}}.\nabla_l \times \mathbf{U} + f)/H] = 0. \tag{2.3}$$

Since the continuity equation implies a streamfunction ψ with $H\mathbf{U} = \hat{\mathbf{k}} \times \nabla_l \psi$, both conservation equations are functions of ψ. Furthermore, letting

$$E = \tfrac{1}{2}(u^2 + v^2) + g(H+\eta)$$

and $\Pi = (\partial v/\partial x - \partial u/\partial y + f)/H$, it can be shown that

$$dE/d\psi = \Pi \quad \text{or} \quad E = E(\psi_0) + \int^{\psi} \Pi \, d\psi. \tag{2.4}$$

Thus, knowing the value of the Bernoulli function on one streamline, the values on the remaining streamlines are determined if Π is known.

The next stage of the approximation is that the cross-stream width of channel varies gradually along the direction of the flow. In this case, the cross-stream velocity u and its derivatives are negligible and so is the y derivative of v. The shallow water equations then reduce to the simple geostrophic relation

$$fv = g\frac{\partial}{\partial x}(H+\eta), \tag{2.5}$$

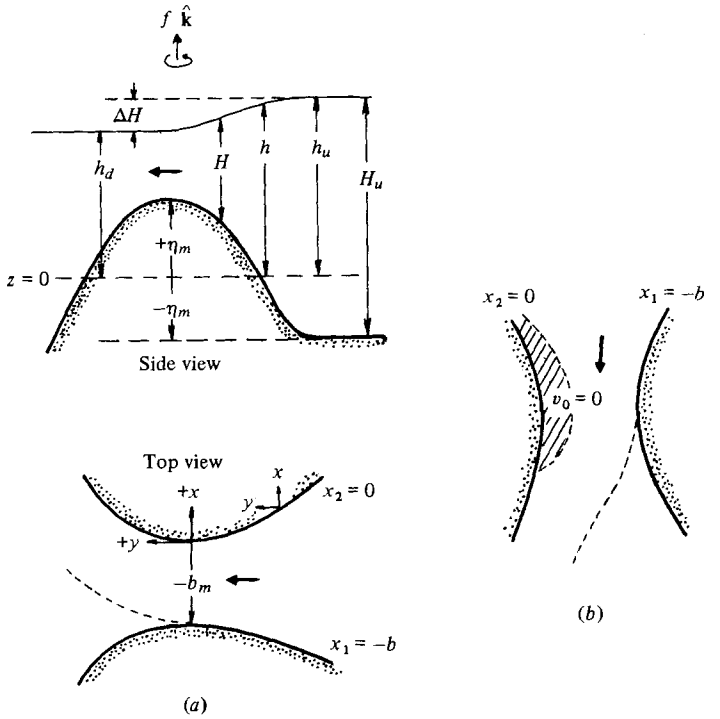

FIGURE 1. (*a*) A sketch of the co-ordinate system and the channel-basin configuration. (*b*) A sketch of the subcritical separated flow, where the shaded area is the stagnant fluid. In (*a*) and (*b*), the short-dashed line is the free streamline separating the current from the fluid in the downstream reservoir.

with the continuity equation replaced by the constancy of the transport,

$$Q = \int_{x_1}^{x_2} vH\,dx = \text{constant}, \tag{2.6}$$

where x_1 and x_2 are at the walls of the channel (figure 1 (*a*)), and the two conservation equations reduce to

$$E_0 = \tfrac{1}{2}v_0^2 + g(H_0 + \eta_0) = \text{constant}, \tag{2.7}$$

$$\Pi(\psi) = (\partial v/\partial x + f)/H, \tag{2.8}$$

where the subscript in (2.7) refers to streamline $\psi_0(x_2 = 0)$. Thus, in their final form, the equations are independent of the downstream co-ordinate y and the flow is to be determined locally at each cross section of the channel. Of course, this does not mean that the flow itself is independent of y. It depends on y implicitly through x_1, x_2 and η. In addition, the flow at each section is related globally through the first integrals, i.e. the conservations of Q, E, and Π.

The foregoing equations generally yield two solutions representing two types of flows, one is the so called subcritical flow which has a speed less than the long-wave speed. The other, the so called supercritical flow, has a speed greater than the long wave speed. The appropriate solution is usually determined by the type of flow specified upstream. However, if the flow speed equals the local long-wave speed at

some section along the channel, then the flow will change character, for example, from subcritical upstream to supercritical downstream, and vice versa. When this occurs the flow is said to be controlled, and the cross section at which the transition occurs is called the control section. The flow having the long-wave speed in this case is called the critical or the controlled flow. In addition to the long-wave speed, a controlled flow is also defined by these additional characteristics: its volume transport is the largest at a given Bernoulli energy, or its specific energy and momentum a minimum at a given transport, and it occurs at the minimum construction (the control section). A summary discussion of these characteristics is presented in the Appendix, where we also give definitions of specific energy and momentum for rotating flows which do not appear to have been previously discussed. For a more formal discussion of hydraulic control, see Gill (1977); also see Stern (1979) for some general principles of control. These characteristics provide the means for computing the control flow and the control section. For the rotating weir problem, we will have the occasion to use them for determining the flow in the weir.

3. Rotating channel flow between two basins

In this section we shall derive theoretical results on rotating channel flow to be tested in the experiment. The model considered here is that of two large basins connected by a channel with fluids flowing from one basin into another through the channel. In this model the free-surface levels of the fluids in the basins will be assumed to be given. The problem is to determine, given these levels, the free-surface height and the velocity of the current in the channel. For comparison with the experiment, the flow will be computed for three cases; the submerged weir-flow, the controlled flow through an irregular channel, and the supercritical separated flow. Each of these will be discussed separately below. But first, as in previous investigations (Whitehead *et al.* 1974; Gill 1977), we assume that the two basins are sufficiently large so that the transfer of fluids between the basins affects the fluid levels in the basins insignificantly and a steady state is maintained. Secondly, all fluid motions in the upstream reservoir are directed toward the channel, i.e. no flow reversal occurs. Thirdly, the flow begins from rest, such as by breaking a 'dam', so that, as the flow settles to a steady state, the potential vorticity everywhere in the upstream basin and in the channel is given by f/H_u and the Bernoulli energy along the right wall looking downstream is given by gh_u, where H_u and h_u are respectively the initial depth and height of the fluid in the basin; here h_u is measured relative to a reference level located midway between the maximum sill height and the floor of the basin (see figure 1(*a*)). The basis for choosing gh_u on the right wall is that the Kelvin wave that signals the initiation of the flow after the dam break has its amplitude confined near the left wall (looking downstream). Hence the surface on the right wall will likely remain at the initial height h_u. Lastly, it will be assumed as usual that the wall and floor of the channel and of the basins vary gradually and smoothly. The case of submerged weir flow is considered first.

3.1. *Submerged weir-flows*

In this problem, the free-surface height of the fluid in the downstream reservoir is above the height of the channel floor. The dependence of the flow on the height of the fluid level downstream will be examined under rotation. For simplicity, the discussion

will be restricted to a channel having a rectangular cross section, i.e. $\eta = \eta(y)$ only.

Since $\Pi(\psi) = f/H_u$, the structure of the flow can be obtained readily from (2.5) and (2.8) which give the depth

$$H = (H_0 - H_u)\cosh \lambda x + v_0(H_u/g)^{\frac{1}{2}} \sinh \lambda x + H_u, \tag{3.1}$$

and the velocity

$$v = (H_0 - H_u)\,(g/H_u)^{\frac{1}{2}} \sinh \lambda x + v_0 \cosh \lambda x, \tag{3.2}$$

where $\lambda = f/(gH_u)^{\frac{1}{2}}$ is the inverse of the Rossby radius of deformation. v_0 and H_0 are the constants of integration representing, respectively, velocity and depth along the right wall $x_2 = 0$ (see figure 1 (*a*) for the co-ordinate system).

Two boundary conditions are obviously required to complete the solution. In the free discharge problem studied here, the boundary conditions are provided by the fluid levels in the upstream and the downstream basins. The application of the upstream condition is straightforward. The fluid level there is easily related to the flow through the Bernoulli function (2.7) along $x_2 = 0$, i.e.

$$gh_u = \tfrac{1}{2}v_0^2 + g(H_0 + \eta), \tag{3.3}$$

since $x_2 = 0$ is a streamline and $E = gh_u$ by assumption.

Relation of the downstream condition to the flow, however, is not trivial, because the fluid discharged into the lower basin differs kinematically from the initially stationary fluid in the lower basin, and so one can no longer use the Bernoulli function or the potential vorticity equation to connect the flow. The lack of a properly posed boundary condition is in fact the central difficulty in the study of the weir flow problem. In this problem, we will assert that the free-surface height of the current on the *left* wall, $x = -b_m$, of the control section (the narrowest section) matches with the fluid level in the downstream reservoir, i.e.

$$H(-b_m) + \eta_m = h_d, \tag{3.4}$$

where $\eta_m = \eta(-b_m) =$ constant, and the subscript m denotes the control section. This matching condition is supported by our experimental observations and also appears reasonable based on physical argument; for example, in Gill's (1976) description of the dam-break problem in a constant depth, straight channel, he showed that following the dam break a Kelvin wave is generated and the current downstream is deflected to the right wall. In the present problem, the flow may be assumed to begin from the same initial state; the flow then would evolve similarly with the deflection of down stream current to the right wall. It thus appears natural that the left edge of the current surface matches with the fluid level in the lower basin. Moreover, for a steady flow evolving from the Kelvin wave, as assumed here, the free-surface height of the flow field everywhere (in the basins and in the channel) cannot be less than the lower basin fluid level, h_d, since this is the minimum surface elevation of the Kelvin wave here. This constraint would further require the matching of the fluid and the current surface to begin at the control section; hence (3.4) follows. (If the height is matched outside the control section, one can easily show by repeating the calculation below that the assumption of a Kelvin wave would be violated.)

Condition (3.4) will be used below for the derivation of the flow field. A qualification to (3.4), however, should be stated: that is, it applies only when the flow in the control

section is subcritical. As will be seen later, this implies that (3.4) is valid only for h above the free-surface height of critical flow. When the flow reaches the critical or the long-wave speed, the flow will become independent of both h_d and (3.4), and at this point, the critical speed will also be the maximum speed that the flow can have in the control section. The reason for this limiting speed is the theoretical result stated in § 2 that the transition from subcritical to supercritical flow can occur only in the narrowest section of a channel in which the flow is critical. In the present problem the flow upstream is always subcritical; according to this result, then the flow can be at most critical and never supercritical in the control (narrowest) section. Hence, the flow speed in the control section is bounded by the critical speed. The following discussion begins with the subcritical flow given by (3.4).

Applying the boundary conditions (3.3) and (3.4) at η_m and $-b_m$, one obtains

$$v_{0m} = -(gH_u)^{\frac{1}{2}} \tanh \lambda b_m + [gH_u \tanh^2 \lambda b_m - 4g\eta_m + 2g(H_u - h_d + \eta_m)/\cosh \lambda b_m]^{\frac{1}{2}}, \quad (3.5)$$

and

$$H_{0m} = (h_u - \eta_m) - v_{0m}^2/2g, \quad (3.6)$$

which give the desired solution at the control section. From H_{0m} and h_d, the transport is also readily computed, since

$$Q_m = (g/2f)\,[H_{0m}^2 - (h_d - \eta_m)^2]. \quad (3.7)$$

With the transport determined at the control section, one can now construct the flow field upstream of the control section. Since the flow profile will be continuously described by (3.1) and (3.2) in the upstream section, it is only necessary to determine the dependence of H_0, v_0 on the geometry by solving for either v_0 or H_0, using (3.3) and the transport relation (2.6). In favour of a simpler expression in terms of v_0, the desired relation is

$$h_u = D(v_0) \coth \lambda b - \left[D(v_0)^2 - 2\frac{f}{g} Q_m\right]^{\frac{1}{2}} \Big/ \sinh \lambda b + v_0^2/2g + \eta, \quad (3.8)$$

where

$$D(v_0) = v_0(H_u/g)^{\frac{1}{2}} + H_u(-1 + \cosh \lambda b)/\sinh \lambda b.$$

In this derivation, a local co-ordinate system for x has been used, i.e. $x = 0$ is always located at the right wall looking downstream (figure 1(*a*)). Equation (3.8) has two roots for v_0, given η and b. In the upstream direction, the appropriate root is the one having $v_0 < v_{0m}$. The upstream flow field given by this root has the appearance of a boundary current, with the volume transport concentrated along the left wall and decaying exponentially into the interior (see Gill 1977 for a detailed discussion of the upstream flow field). It should be remarked that (3.8) is applicable only from the upstream to the control section. The downstream current is fixed by the fluid level of the lower basin, and the geometrical dependence in (3.8) becomes irrelevant. It should also be noted that the first two terms on the right-hand side of (3.8) are also the expression for H_0, which has to be real and positive for (3.8) to be valid. The appearance of the square-root sign thus requires that $D(v_0)^2 - 2fQ_m > 0$, or

$$V_0(H_u/g)^{\frac{1}{2}} + H_u(-1 + \cosh \lambda b)/\sinh \lambda b > 2fQ_m/g.$$

The inequality is satisfied only if b increases sufficiently rapidly relative to the decrease of v_0 in the upstream direction.

Equation (3.8) together with (3.5) and (3.6) complete the solution of subcritical weir flow between two large basins. As stated earlier, the maximum speed that this flow can have is the critical or long-wave speed. This limiting speed can now be obtained from (3.8) using one of the critical flow criteria summarized in § 2, namely, minimization of specific energy. In the present problem, this is equivalent to minimizing (3.8) with respect to v_0 at the control section, i.e. $\partial(h_u-\eta)/\partial v_0 = 0$, at η_m. The result is

$$V_0^4 - \frac{2(gH_u)^{\frac{1}{2}}}{\sinh\lambda b} V_0^3 - 2\left(\frac{fQ_m}{H_u}\right) V_0^2 - \left(\frac{fQ_m}{H_u}\right)\frac{(gH_u)^{\frac{1}{2}}}{\sinh\lambda b} V_0 - \left(\frac{fQ_m}{H_u}\right)\frac{f^2b^2}{\sinh\lambda b} = 0, \qquad (3.9)$$

where $V_0 = v_{0m} - (1-\cosh\lambda b)(gH_u)^{\frac{1}{2}}\sinh\lambda b$. From this equation the speed is determined by eliminating the transport Q_m with the aid of (3.8). (No closed form for v_{0m} can be obtained, however. With regard to the critical flow, reader may wish to refer to Gill's paper (1977) for additional details of the flow not discussed here; an expression of critical height is also given in his paper.) The subcritical speed given by (3.5) varies inversely with the downstream level, h_d. Thus, as remarked at the beginning of the discussion, the limiting critical speed also implies a minimum downstream level, below which the flow will be unaffected by h_d. This departure from the downstream condition (3.4) will be useful later in the experiment for it provides a convenient means for identifying the transition from subcritical to critical flow.

Equations (3.5) to (3.7) and (3.9) express speed, free-surface height, and transport as functions of h_u, $h_d f$ and H_u. Although the equations can now be examined for effects of these parameters on flow properties, the equations are not uniformly valid for all parameter values. The limitation arises from our assumption of no flow reversal for free-discharge flow. This assumption requires $v_{0m} \geqslant 0$ at all times. The condition for vanishing v_{0m}, given by equating the sum of the last two terms in (3.5) to zero, is

$$\cosh\lambda b_m - (\Delta H + 2\eta_m)/2\eta_m = 0, \qquad (3.10)$$

where $\Delta H = h_u - h_d$ and $H_u - h_d = \Delta H + \eta_m$ have been used. The flow reversal occurs, on the other hand, when the sum of the last two terms in (3.5) or, equivalently, the sum of the two terms on the left-hand side of (3.10) becomes negative. Thus, for the equations to be valid under the no-flow-reversal condition, the parameters f and H_u clearly must not be greater than, and ΔH not less than, the values of their respective roots in (3.10).

The no-flow-reversal condition here has limited the range of parameter values to which Equations (3.5)–(3.9) can be applied. However, it will be possible to extend the steady-state solution beyond the ranges of values stated above and still to satisfy the no-flow-reversal condition. This can be achieved if we relax a requirement which has been implicitly assumed in the calculation so far: namely, the requirement that the flow occupies the full width of the channel. The extension of the steady-state solution is possible after the removal of this constraint because the parameter values which previously produce flow reversal can now be made to satisfy the condition of no reversal, (3.10), by using a smaller value of b_m. In other words, rather than fix the width of the current to the full width of the channel, the width b_m is treated as the width of the current and allowed to decrease so as to satisfy (3.10). The narrowed

current is assumed here to be supported by a pool of stationary fluid which fills the portion of the channel not occupied by the current; the position of the stationary fluid is to the right of the current so that the pressure and velocity can be continuous across the free streamline separating the current and the fluid. Therefore, a picture of the complete flow field would look like the sketch in figure 1(*b*). The current with reduced width may be referred to here as 'separation' flow for its detachment from the right channel wall. The separation flow with a stagnant fluid region described above appears to be the only solution possible under the assumptions of steady state and no flow reversal, for parameter values outside the range of applicability of Equations (3.5)–(3.9). We shall assume the existence of the separation flow and incorporate this flow into the total solution of the channel flow for later comparison with experiments. (There are some difficulties, nevertheless, with the separation-flow solution in that the stagnant fluid region supporting the current may or may not be realizable from an initial state and that the free streamline separating the current and the stationary fluid may be unstable to perturbations. Where difficulties may be encountered will be indicated in the discussion.)

There are two cases of separation flow, and it is convenient to distinguish the two for later comparison with experiments. The first case may be called 'subcritical' separation where the lower basin level h_d is always above the sill height η_m and the flow is subcritical. For this case, the transport is given by

$$Q_m = (g/2f)\,(h_u^2 - h_d^2), \tag{3.11}$$

with $v_{0m} = 0$.

The other case may be called 'critical' separation where h_d is always below the sill height η_m and the flow is critical. This case has been previously discussed by Whitehead *et al.* (1974) and Gill (1977). It differs from subcritical separation in that the free surface always intersects the left corner of the channel floor, i.e. $H(-b_m) = 0$; otherwise, the flow field looks similar to figure 1(*b*). However, the critical separation flow may be quite unstable since the drop of the current surface downstream of the control section does not appear to be able to support the level surface of the stagnant fluid. This point will be verified in the experiment.

The solution for submerged weir flow through a rectangular channel is now essentially complete, and the flow field can be examined for all values of h_u, h_d, f and H_u. The main effects of the rotation f are seen here to be twofold: first, to reduce flow speed and transport, and second, to bring in the upstream influence, namely H_u the fluid depth of the upper basin. The latter tends to reduce the flow further; in other words, shallow upstream fluid depth H_u produce smaller transport and speed. In addition to these two effects, rotation also produces velocity shear in current which may lead to the flow separation discussed above. If this occurs, the effects on transport are still the same but the width of the current decreases with increasing f and H_u, with v_{0m} remaining at zero. As to the effects of the other two parameters, increasing h_u or decreasing h_d always leads to an increase in speed and transport except that critical flows are unaffected by h_d as already indicated. So their effects on the flow are similar to those found in non-rotating weir flow. Lastly, it may be mentioned that the effect of channel width b_m, not discussed so far, is similar to that produced by rotation on the non-separated flow. This should be apparent as b_m often occurs in combination with f.

3.2. *Controlled flow through a channel of irregular cross section*

This sub-section is concerned with the influence of the cross-channel geometry on controlled flow. The discussion will be restricted to the controlled flow having zero potential vorticity. This case allows fairly general channel geometry to be examined without unnecessary complication. The case is also most easily and accurately measured experimentally. The actual channel employed in the experiment is a 'truncated' channel which has two vertical walls and a straight slanting floor across the width of the channel. The properties of the flow in this channel are easily deduced from the general results presented here and will be briefly discussed at the end.

For a zero potential vorticity flow, i.e. $\lambda \to 0$, (3.1) and (3.2) have the asymptotic forms, respectively,

$$h = \frac{-f^2}{2g} x^2 + \frac{f}{g} v_0 x + h_0, \tag{3.12}$$

and

$$v = -fx + v_0, \tag{3.13}$$

where the depth H in (3.1) has been replaced by h, the free-surface height. The Bernoulli function remains the same as (3.3). But the transport of the flow becomes

$$\begin{aligned} Q &= \int_{-b}^{0} v(h-\eta)\, dx \\ &= \left(\frac{fb}{2} + v_0 b\right)\left(h_0 - \bar{\eta} - \frac{f^2 b^2}{4g} - \frac{fbv_0}{2g}\right) + fb\overline{\overline{\eta'}}, \end{aligned} \tag{3.14}$$

where $\bar{\eta}$ is the mean elevation, $\bar{\eta} = (1/b)\int_{-b}^{0} \eta\, dx$, η' is the deviation from the mean, $\eta' = \eta - \bar{\eta}$, and $\overline{\overline{\eta'}}$ is the moment of the deviation, $\overline{\overline{\eta'}}(1/b) = \int_{-b}^{0} x\eta'\, dx$. It should be noted that for a completely general geometry such as the one depicted in figure 2(*a*), the width b will be a function of the flow speed. Only for the special case in which the channel has straight vertical walls is the width constant. Therefore, the mean elevation mentioned above applies only to that part of the channel boundary in contact with the fluid.

Before computing the controlled flow, it is worthwhile to point out a close analogy between the zero potential vorticity flow and the non-rotating flow. The analogy is most easily shown using the zero-potential-vorticity form of (3.8), which can be obtained by eliminating $h_0 (= H_0 + \eta_0)$ in the Bernoulli function (3.3) with (3.14). The resulting equation is

$$gh_u = \frac{g(Q - fb\overline{\overline{\eta'}})}{b(fb/2 + v_0)} + (fb/2 + v_0)^2/2 + f^2b^2/8 + g\bar{\eta}. \tag{3.15}$$

Now make the transformation $E_* = gh_u - \frac{1}{8}f^2b^2$, $Q_* = Q - fb\overline{\overline{\eta'}}$, and define an average velocity $\bar{v} = (1/b)\int_{-b}^{0} v dx = \frac{1}{2}fb + v_0$, the equation reduces to

$$E_* = gQ_*/b\bar{v} + \bar{v}^2/2 + g\bar{\eta}. \tag{3.16}$$

One recognizes this as just the familiar Bernoulli function for describing speed variation in a non-rotating channel (for example, see Rouse 1961). Thus, the effect of rotation is to reduce E and Q (if $\overline{\overline{\eta'}} > 0$). Otherwise, the flow varies with the geometry in a way similar to non-rotating flow. In fact, the formula for the speed of the controlled flow is nearly identical with that of the non-rotating case as will be evident below.

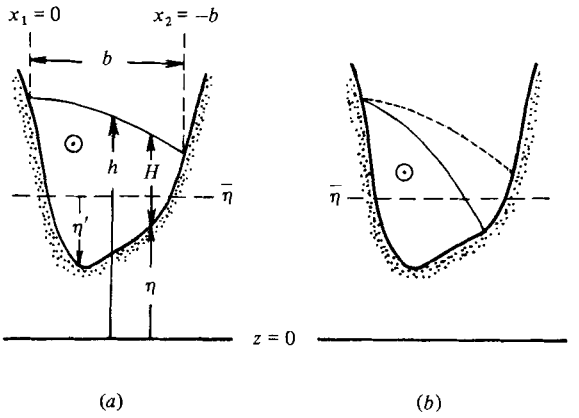

(*a*) (*b*)

FIGURE 2. (*a*) A cross-sectional view of an irregular channel. (*b*) The free-surface profile for a separated flow (solid curve) and a non-separated flow (dashed curve).

The controlled flow can now be obtained by minimizing either (3.14) or (3.15) with respect to v_0. In view of the possibility that b may be a function of v_0, it is simplest to maximize the integral form of the transport in (3.14) directly. Substituting (3.12) and (3.13) for v and h respectively in (3.14), replacing h_0 with $gh_u - v_0^2/2g$ and using the fact that $H(0) = H(-b) = 0$ if the channel wall is not vertical, one has

$$\partial Q/\partial v_0 = 0 = \int_{-b}^{0} (v^2 - gH)\, dx, \tag{3.17}$$

from which follows the average critical speed

$$\bar{v}_c = (2/3)^{\frac{1}{2}} (E_* - g\bar{\eta})^{\frac{1}{2}} = (2/3)^{\frac{1}{2}} [g(h_u - \bar{\eta}) - f^2 b^2/8]^{\frac{1}{2}}. \tag{3.18}$$

Substitution of $\bar{v}_c$ in (3.16) gives the transport of the controlled flow,

$$Q_c = (b/g)\,[2(E_* - g\bar{\eta})/3]^{\frac{3}{2}} + fb\overline{\overline{\eta'}}. \tag{3.19}$$

The shorter form of $\bar{v}_c$ in (3.18) is also the form for the speed of non-rotating critical flow. Equations (3.18) and (3.19) are general formulae for the zero-potential-vorticity controlled flow. As one can see, the speed of the controlled flow is independent of the channel geometry. It is the mean elevation and the width of the channel that determine the critical speed. The geometry, however, does affect the transport. The irregularity of the channel floor can increase or decrease the transport depending on the sign of $\overline{\overline{\eta'}}$. It can be stated approximately that if the channel is deeper (shallower) on the average near the left wall, $\overline{\overline{\eta'}}$ is likely to be positive (negative) and the transport increases (decreases). The physical explanation is that the speed of the flow is greatest near the left wall. Since positive (negative) $\overline{\overline{\eta'}}$ usually implies greater (lesser) depths near the left side of the channel, the transport increases (decreases) accordingly. In the case of the symmetrical channel, $\overline{\overline{\eta'}}$ will be identically zero if the free surface intersects both vertical walls, and it will be positive if the free surface intersects any part of the channel contour which is not vertical or the channel has no vertical walls at all. The reason for the former is self-evident. For the latter case, the channel is always deeper on the average near the left edge of the flow.

The above results have been obtained for the zero-potential-vorticity flow. The

results are probably qualitatively similar in the finite-potential-vorticity case since the flow will also have a negative shear even though it may be depth dependent. In this case, a deeper floor on the left part of the channel should also result in a larger volume flow.

The foregoing discussion has assumed that $v_0 > 0$. When the rotation and the upstream height are such that

$$f^2b^2 = 2g(h_u - \overline{\eta}), \tag{3.20}$$

v_0 can also become zero as can be seen from (3.18). In the case of the rectangular channel, $v_0 = 0$ is marked by the intersection of the free surface with the floor, which leads to separation of the flow. In an irregular channel, a simple geometrical distinction between the floor and the wall no longer exists. The intersection of the free surface with the boundary of the channel does not necessarily imply $v_0 = 0$ nor that the separation takes place. The aim here is to show that the separation as defined by $v_0 = 0$, can be achieved if $H(-b) = \eta(-b) \leqslant \overline{\eta}$, and no separation occurs if

$$H(-b) = \eta(-b) > \overline{\eta}.$$

In this latter case, the floor acts as a 'wall'.

The result can be most easily shown by assuming first that $v_0 = 0$. The rotation at which this occurs is then given by (3.20). The free-surface height at the left wall is given by (3.12),

$$h(-b) = -f^2b^2/2g - fbv_0/g + h_0.$$

Substituting (3.20) into $h(-b)$, setting $v_0 = 0$ and replacing h_0 with h_u, the height along the left wall is simply

$$h(-b) = \overline{\eta},$$

which is the depth of the fluid at hypothetical separation. The actual height of the surface at the intersection with the floor is $\eta(-b)$. Thus, if $\eta(-b) \leqslant \overline{\eta}$, v_0 will certainly approach zero (figure 2(*b*)). On the other hand, if $\eta(-b) > \overline{\eta}$, this would imply that the surface intersects the floor before v_0 becomes zero. Hence there cannot be a separation.

In the experiment, the above results will be verified with a truncated channel. The floor of this channel is described by $\eta = \overline{\eta} + (x + \frac{1}{2}b)\,s$ and it has the moment $\overline{\overline{\eta}'} = \frac{1}{2}sb^2$, where s is a constant. For this channel the volume transport is just

$$Q = (b/g)\,[\tfrac{2}{3}(gh_u - g\overline{\eta} - \tfrac{1}{8}f^2b^2)]^{\frac{3}{2}} + \tfrac{1}{12}sfb^3. \tag{3.21}$$

(For $s = 0$, the equation reduces to that given by Whitehead *et al.* 1974). Thus, the transport is larger for positive s, where the floor and the free surface of the current slope are in the same direction. As to the effect of rotation, Q generally decreases with rotation. But, for positive s, (3.21) also can be shown to increase at some moderate rotations. The rotation at which Q attains a maximum is given by

$$f^4 - 8gb^{-2}(h_u - \overline{\eta})f^2 + \tfrac{4}{3}g^2s^2b^{-2} = 0.$$

The experiment will verify this pattern of dependence of the transport on f and s.

3.3. *The supercritical separation*

The previous two cases dealt with the subcritical and critical flows and it was shown that both flows under some conditions would separate from the channel wall. In the

following, the supercritical flow will be examined for separation. This case is of interest because, unlike the previous two, the separated flow will be deflected to the right wall and the position of the separation can be easily visualized and measured in the experiment.

For this problem a rectangular channel will be used and it will be assumed that the level floor of the channel extends into the downstream basin, so that the only change in geometry downstream is the gradual widening of the channel wall. It will further be assumed that the downstream basin is empty so that the flow at the control section is always critical and the downstream flow is supercritical.

Since the downstream section now represents essentially an ever widening channel (again consider only the zero-potential-vorticity case), the change of the flow downstream can be described by (3.15). It is easily shown using (3.15) that as b increases, v_0 increases and the free surface will eventually intersect the floor, i.e. $H(-b) = 0$. Rather than computing the entire downstream field, we shall show the existence of the separation by directly computing the width at which the flow separates.

At the point of separation, h at the left wall vanishes, and the condition at $x = -b$ is $0 = -(f^2b^2/2g) - (fb/g)\,v_0 + h_0$ from (3.12). The vanishing of $h(-b)$ also means that Q is equal to $(g/2f)\,h_0^2$. Solving for v_0 from the above two equations gives

$$v_0 = -\tfrac{1}{2}fb + (2fgQ)^{\frac{1}{2}}/fb.$$

By eliminating v_0, (3.12) becomes

$$gh_u = (\tfrac{1}{2}fgQ)^{\frac{1}{2}} + (gQ/fb^2) + \tfrac{1}{8}f^2b^2. \tag{3.22}$$

But h_u is related to Q, since the transport is determined by the critical flow in the channel. Let b_m denote the width of the control section. H_u is related to Q by

$$gh_u = \tfrac{1}{8}f^2b_m^2 + \tfrac{3}{2}(gQ/b_m)^{\frac{2}{3}}.$$

Using this value of gh_u in (3.22), and after some rearranging of terms, the width of the current downstream at which the separation occurs is thus obtained by solving

$$b^4 + \left[\frac{4}{f^2}(2fgQ) - b_m - \frac{12}{f^2}(gQ/b_m)^{\frac{2}{3}}\right] b^2 + \frac{8gQ}{f^3} = 0. \tag{3.23}$$

Clearly the width will be a function of the rotation. It is straightforward to show that it decreases monotonically with increasing rotation. In a flared channel, the decrease in width means that the separation point moves upstream toward the control section. As the point reaches the control section, the supercritical separation and the critical separation become indistinguishable.

4. The experiment

The experimental apparatus is basically similar to the one used by Whitehead *et al.* (1974); the two basins are constructed by dividing a right circular cylinder in half with a vertical partition, and the weir is constructed from a short section of the channel, 7·5 cm long and 4·4 cm wide, plaed between the two basins and across the partition (see figure 3). There are, however, two modifications in our experiment. One is the smoothing of the channel entrance; in particular, the left wall of the entrance is made smooth by extending it upstream and making it part of the basin boundary (Figure 3, top view).

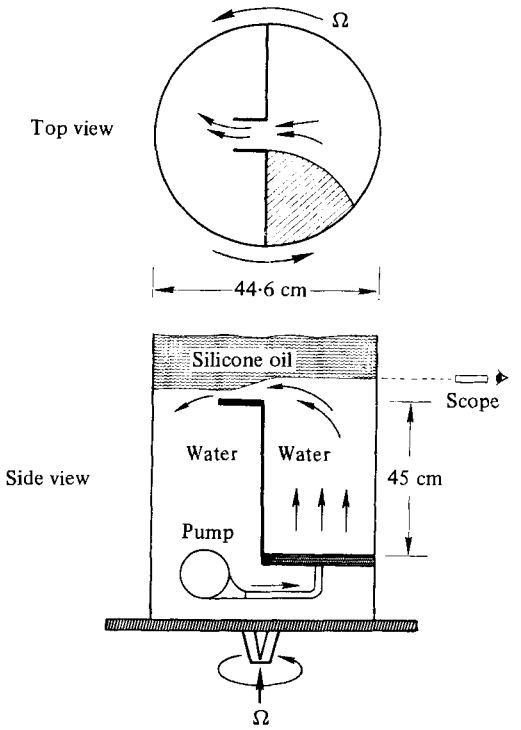

FIGURE 3. A sketch of the apparatus.

Smoothing of this wall is important because the experiment shows that the floor in the channel is fed by the boundary current along the left wall. A sharp entrance wall can interfere with the flow – a fact confirmed by the experiment – and is to be avoided. The other modification is in the recirculation system. In order to maintain the flow in a steady state, the fluid discharged into the downstream basin must be recirculated back upstream. In our experiment, the fluid is recirculated back through the bottom of the floor with the floor, composed of simple porous materials such as wire mesh and sponge, acting as a diffuser. This method of recirculation allows the fluids to well up into the basin more evenly. We also put in a second fase bottom which is made of cheesecloth stretched on a rigid frame. This porous floor spreads the upwellings further. It also provides a smooth bottom and can be raised up and down to adjust the depth of the reservoir. A final small but useful improvement of the experiment is the coating of a thin film of nonwetting silicone grease to the walls and floor of the channel. The coating prevents 'sticking' of the water to the channel wall due to surface tension – a problem that can seriously hinder the observation of the separated flows.

Our apparatus is mounted on a turntable with a variable speed drive. The experimental procedure involves adjusting the rotation rate and the pumping rate (which essentially gives the transport of the flow), and then measuring the height of the free surface in the two basins. The height is measured through a telescope with an accuracy of $\pm$ 0·01 cm. The rate of discharge is measured with a flow meter connected to the submersible pump. The meter measures from 2·0 litres per minute (l/min) to 22·7 l/min with an accuracy of $\pm$ 0·08 l/min. The meter is mounted vertically along the axis of rotation so that the centrifugal force on the meter is minimized. The rotating turntable

is driven by a variable speed motor with $\pm 0{\cdot}01$ s/rev accuracy. The table is also carefully levelled before the experiment; the static tilt of the axis of rotation from the local gravity is no more than 10^{-3}. The fluid used for the experiment is basically water. A passive layer of silicone fluid, specific gravity 0·916, is usually placed on top of the water whenever the effect of reduced gravity, defined as $g' = g\Delta\rho/\rho$, is desired, where $\Delta\rho$ is the density difference between the two fluids and ρ is the density of the working fluid. The value of the reduced gravity can be adjusted by mixing an appropriate amount of alcohol with the water. The density is measured with a hydrometer, which has an accuracy of $\pm 0{\cdot}002$.

In the experiment, no attempt is made to measure the structure of the current. The current speed is too fast ($\sim$ 20 cm/s) to allow it to be measured confidently. But some visual observations of the flow field are obtained and can be compared qualitatively with the theory. The quantitative comparison is presented in the next section.

4.1. *Observations*

In the channel, the feature of the current most easily observed is the tilt of the free-surface height of the current. Observation shows that the surface slope increases with rotation, and at high rotation the surface intersects the floor just as predicted by the theory. At still higher rotation, we are able to observe critical and supercritical separations (figures 4 and 5, also see next section for more details). The observation of the subcritical separation flow at low discharge rate is, however, not conclusive. Colour dyes are also injected to observe the speed of the current in the channel. The greatest speed is found near the left wall, implying a negative shear which agrees with the theory. The dye also shows a generally laminar current. The flow can, however, become somewhat unsteady at high rotation and large flow rate.

In the upstream basin a large anticyclonic circulation covering the basin and a narrow boundary current along the left basin wall are observed.† The anticylonic circulation is weak ($\sim$ 0·5 cm/s) whereas the boundary current which branches off from this interior circulation is rather swift ($\sim$ 10–20 cm/s). The principle role of this boundary current is seen to transfer the upstream fluid through the channel into the lower basin. The presence of such a boundary current on the left wall has been previously predicted theoretically. Observation seems to confirm this prediction. But the attempt to compare the width of the current with the Rossby radius of deformation is not successful owing to interference by the gyre. The contribution of the anticyclonic velocity in the gyre to the upstream Bernoulli function is insignificant; it is less than 0·1 %. The contribution to the potential vorticity is also small – less than 1 %.

In the lower reservoir, special attention is paid to observing the merging of the free surface of the current with that of the reservoir. It has been argued in the theory that the surface height of the current on the left wall of the control section should merge with the fluid level of the lower reservoir when the level downstream is above a certain critical height. When it is below this height, the flow in the control section should be

† The picture reminds one of the subtropical gyre and the western boundary current. But the resemblance is only superficial. A simple test such as tilting the floor of the basin shows that a sloping floor, the equivalent of the variable coriolis parameter in the ocean, has no effect on the formation of the boundary current.

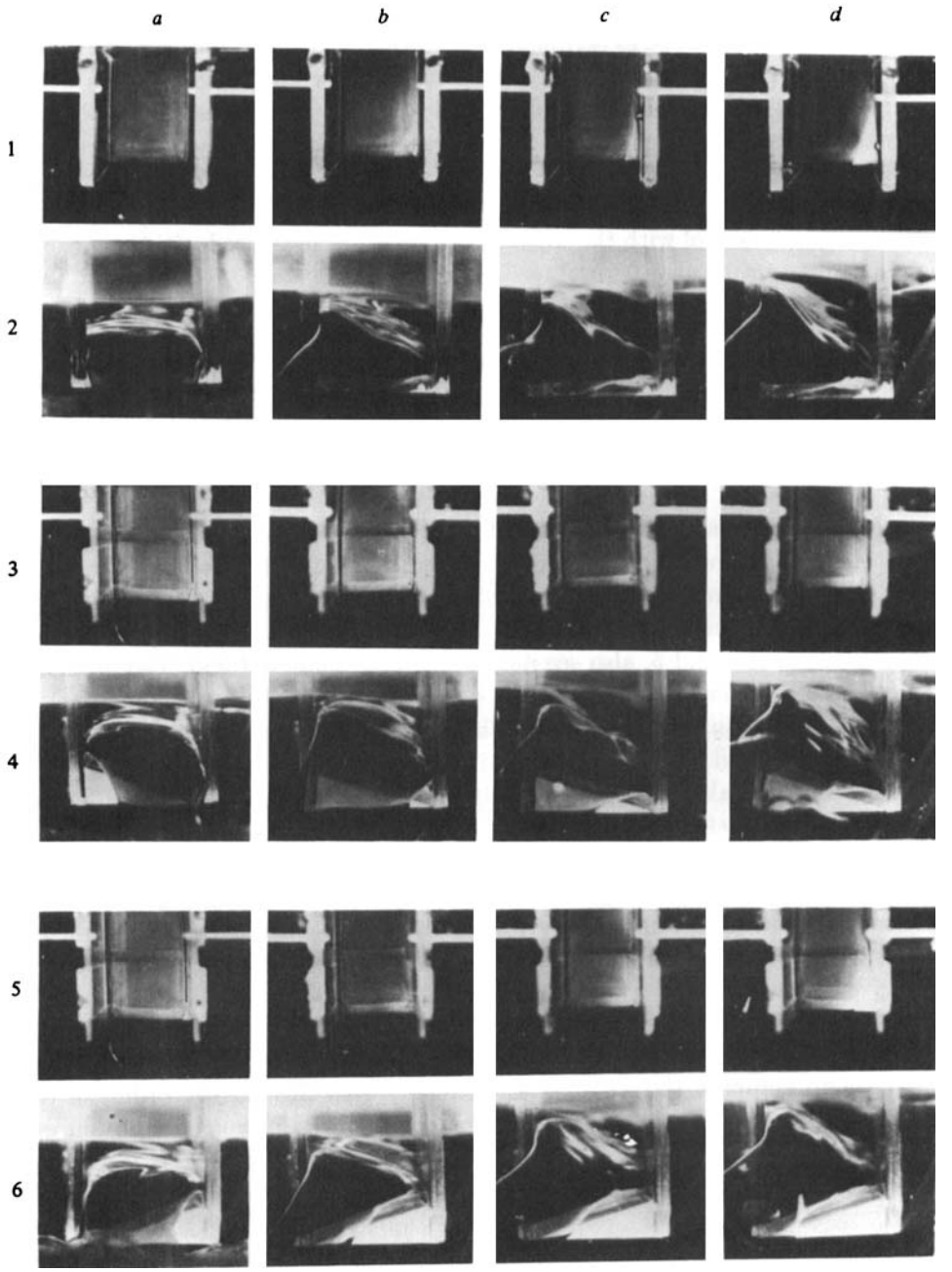

FIGURE 4. Top view and front view of zero-potential-vorticity flows in a rectangular channel (rows 1 and 2, $\beta = 0$) and two truncated channels (rows 3 and 4, $\lambda = 0{\cdot}29$; rows 5 and 6, $\beta = -0{\cdot}18$). The frequencies of the rotation for the four frames on each row are (*a*) $f = 0{\cdot}0$ rad/s, (*b*) $f = 3{\cdot}60$ rad/s, (*c*) $f = 6{\cdot}28$ rad/s, and (*d*) $f = 8{\cdot}38$ rad/s. The odd-numbered rows are the top views. In each of the top views, the outline of the channel is given by the two parallel white bars. The direction of the flow is from top to bottom. Note the deflection of the current to the left of the picture as the rotation rate increases. The white area near the right side wall of the channel shows where the current has separated and it is not occupied by the current. The even-numbered rows are the front views. The flow is out of the page. The tilt of the free surface is clearly visible.

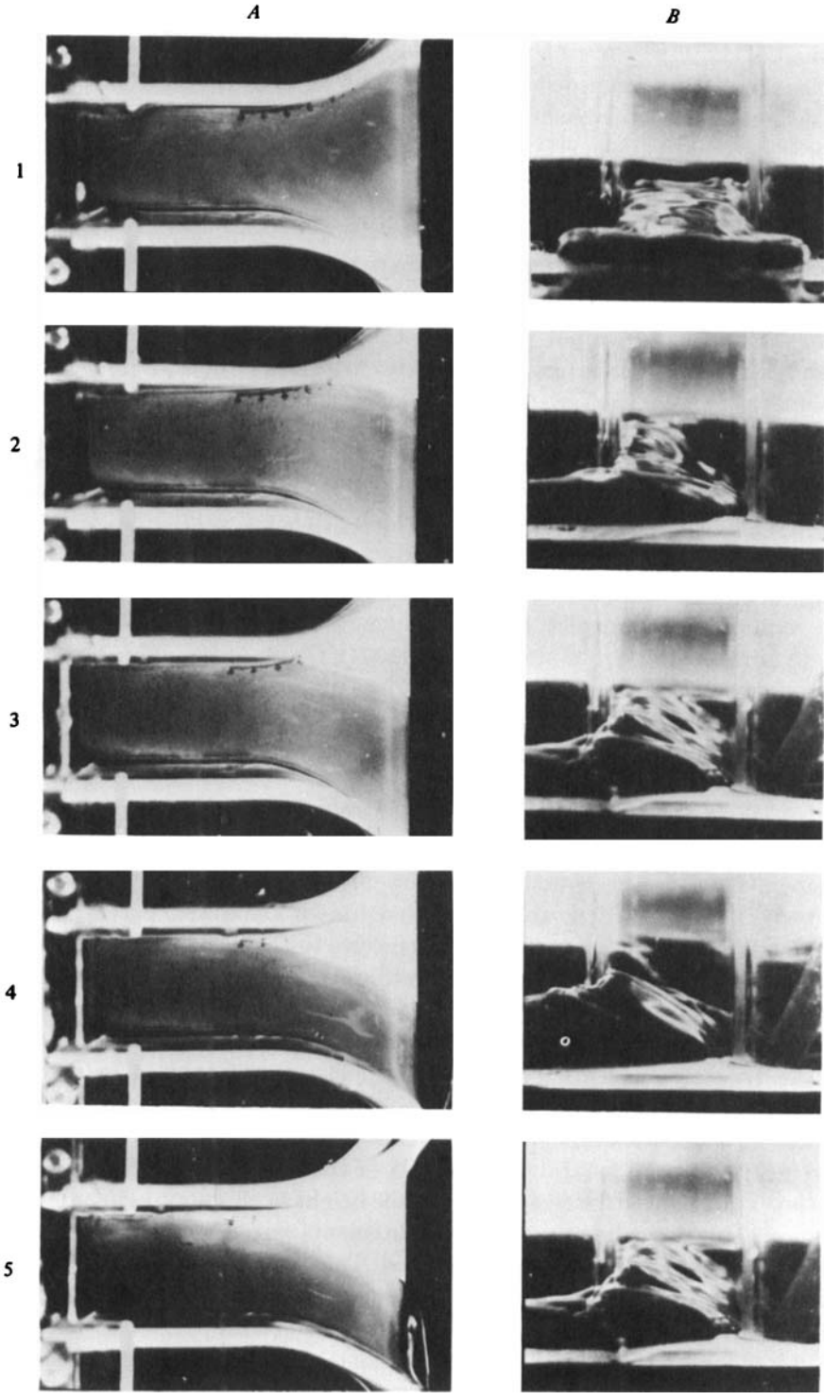

FIGURE 5. Top view and front view of zero-potential-vorcitity flow in a flared rectangular channel. Column A shows the top view, in which the current flows from left to right. Column B shows the front view, in which the flow is out of the page. The frequencies of rotation f are (1) 0·0, (2) 1·58, (3) 3·14, (4) 6·28 and (5) 7·0 rad/s. In the front view, the current is marked by the dark colour dye. The area unoccupied by the current appears white. The separation of the current from the wall is visible and note its upstream movement with increasing rotation rate.

independent of the downstream level. In the experiment, such matching conditions are indeed observed; the current deflects to the right wall as it leaves the control section, and the surface on the left edge of the current follows the fluid level of the lower basin whenever the downstream level is high. When the level is low, the surface height of the current ceases to follow it and remains unaffected by the level of the lower reservoir.

5. Comparisons between Theory and Experiment

An important step in the data reduction is normalizing the measured transport with respect to some reference value – principally the transport of the critical flow. In this experiment, the measured transport is consistently lower than predicted. Normalization helps to remove such systematic offset and still allows measurements to be compared with theory. The lower transport measured is believed to be caused by friction. Evidence of this is the observed small downstream decrease in the free-surface height along the channel – an indication of the loss of pressure head (and hence transport) due to friction. Some estimate of the possible loss is also obtained based on a simple viscous boundary layer consideration (see figure 6 and its caption), and the percentage of loss is consistent with what has been measured. It should be mentioned that the reduction of transport by friction has been long noted in classical open-channel hydraulics (for example, Houton 1907; Chow 1959). The percentage of reduction given in classical hydraulics for similar parameters is about the same as that observed in our experiment. Bearing this in mind, we present comparisons between theory and experiments for the three cases.

5.1. *The submerged weir-flow*

There are two sets of measurements involved in the experiment; one is used to compare the transport for different potential-vorticity flows, and the other to compare the transport at different rotations and surface heights for a non-zero potential-vorticity flow. The latter measurements are quite insensitive to the depth change of the upper reservoir and allow a wide range of rotation rate and transport to be examined. We will consider this case first. For this case, the actual potential vorticity given by λb_m is about 0·1, but may be regarded as zero since its transport differs by only 0·1 % from that of the true zero-potential-vorticity flow. The experiment is carried out by measuring the upstream and downstream free-surface height for different increments of transport at a fixed rotation rate. (For convenience, the free-surface heights are measured relative to the maximum elevation of the channel floor. Such a choice of reference level will be used for measuring surface height in all the experiments reported in this paper.) This procedure produces measurements through two flow regimes, sub-critical to critical, as the transport is increased. The two regimes are distinguished in the experiment by watching for the occurrence of a drop in the free-surface height at the mouth of the channel. According to the theory, such a drop signals a critical flow. In order to compare the measurements with the theory as well as to distinguish the two regimes, all transports are normalized with respect to the transport at which the flow is just critical (the actual value of this critical transport is shown in figure 6(*b*) as a percentage of the expected value). These normalized values are then plotted as a function of the upstream height. The plot, with the values indicated by cross-error bars, is shown in figure 7, where h'_u is the dimensionless height obtained by dividing the

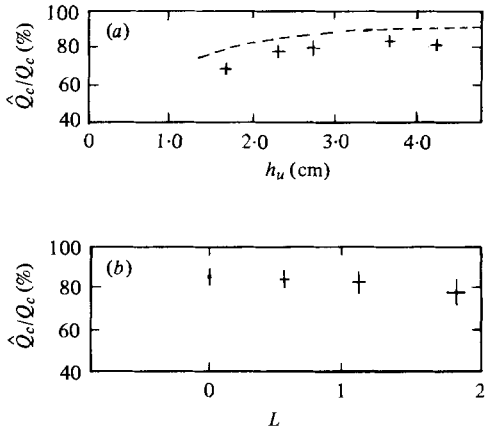

FIGURE 6. Percentage of the measured transport $\hat{Q}_c$ to the theoretical transport Q_c, (*a*) as a function of the upstream height h_u for the non-rotating controlled flow, and (*b*) as a function of the rotation $L = fb/(g'h)^{\frac{1}{2}}$ for the rotating controlled flow used in figure 7. In (*a*), the dashed line is the estimated ratio between the theoretical transport and the transport based on a simple viscous boundary-layer consideration; let the layer be approximated by $\delta = [\nu l/(2g'h_u)^{\frac{1}{2}}]^{\frac{1}{2}}$, where $\nu \simeq 0{\cdot}01$ cm^2/s is the kinematic viscosity, $l = 7{\cdot}5$ cm is the length of the channel, and $(2g'h_u/3)^{\frac{1}{2}}$ is the approximate speed of the flow with $g' \simeq 82$ cm/s^2. The ratio of the cross-sectional area of the flow excluding the viscous layer to the uncorrected area is about $(1-3\delta/h_u)(1-2\delta/b)$ assuming viscous layers on these walls of the channel and at the interface. Another 2% may be subtracted from this ratio to account for the capillary effect at the walls. The dashed line is the final ratio for different h_u.

measured height h_u by $\bar{h}$, the mean height between the two basins, and $L = fb/(g'\bar{h})^{\frac{1}{2}}$ is the dimensionless rotation rate. Note that only the dependence on h_u is given because the total fluid volume of the two basins is conserved, which allows h_d to be related to h_u by $h_d = 2\bar{h} - h_u$. On the same figure, the theoretical curves of transport against upstream height are plotted as solid lines: the dash lines mark the theoretical boundaries of the flow regimes. The formulae for these curves are given by the zero-potential-vorticity form of (3.7), which corresponds to (3.21) with zero s and $\bar{\eta}$, for non-separated flows, and (3.11) for separated flows. A listing of the formulae grouped according to flow re imes *along* each curve is shown in table 1, where the formula has been non-dimensionalized as indicated above as well as normalized. The normalizing factors D_1 and D_2 in the table are the dimensionless critical transport predicted from initial $\bar{h}$, f and b, or simply L, using (3.21) and (3.11), respectively.

As one can see from figure 7, there is a general agreement between theory and experiment. At zero rotation, which is the classical weir-flow case, the agreement is quite reasonable especially in the mid and low range of transport. At higher transport, the measured value is somewhat lower which indicates a possible need for higher frictional corrections. For the rotating flow, the agreement again looks acceptable except perhaps for the case of rapid rotation, $L = 1{\cdot}865$. At this high rotation rate the fluid surface in the reservoir becomes wavy and measurements become less accurate. The lack of measurements at low transport is due to the very low pumping rate required, which cannot be monitored with our flow meter. This lack of measurements has prevented us from verifying satisfactorily the subcritical separation flow. Only two measurements at $L = 1{\cdot}132$ can be made in the subcritical separation regimes, and agreement with the theoretical curve is marginal.

	$L < 2$	$L \geqslant 2$
I. Critical	$(2h'_u/3 - L^2/12)^{\frac{3}{2}}/D_1$	$(2h'_u/3 - L^2/12)^{\frac{3}{2}}/D_2$
II. Subcritical	$[2(h'_u - 1)^{\frac{1}{2}} - L/2]\,[2 - h'_u + L(h'_u - 1)^{\frac{1}{2}} - L^2/4]/D_1$	—
III. Subcritical with separation	$2(h'_u - 1)\,L^{-1}/D_1$	$2(h'_u - 1)\,L^{-1}/D_2$
IV. Critical with separation	—	$2(4h'_u)^2\,L^{-1}/D_2$

$$D_1 = (\tfrac{2}{3})^{\frac{3}{2}}\left[\frac{6}{5} + \frac{2L^2}{25} + \frac{3L^2}{25}(5L^{-2} - \tfrac{1}{4})^{\frac{1}{2}} - \frac{L^2}{8}\right]^{\frac{3}{2}}, \quad D_2 = L^3/8.$$

TABLE 1. Transport formulae for the curves in figure 7.

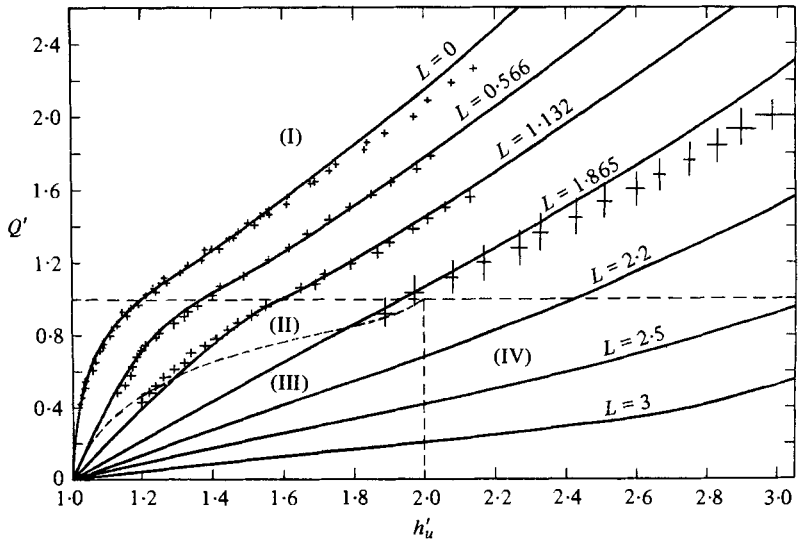

FIGURE 7. Transport, $Q' = Q/Q_{ci}$, of zero potential vorticity, submerged flows versus upstream height, $h'_u = h_u/\bar{h}$, at various rotations $L = fb/(g'\bar{h})^{\frac{1}{2}}$. Q_{ci} is the critical transport at the transition from the subcritical to the critical flow. $\bar{h}$ is the mean height of the fluid between the two basins. The solid lines are the theoretical curves, see table 1 for the formulae of the curve. The dash lines are the boundaries of the flow regimes: (I) critical, (II) subcritical, (III) subcritical with separation, and (IV) critical with separation. The crosses denote the measurements. The length of the bar is the uncertainty of the measurement.

The next set of measurements is for comparison of different potential-vorticity flows. We choose to compare the transport of the different potential vorticity flows at a given upstream height. For the submerged-weir-flow experiment, this means fixing the upstream height and varying the downstream height. The required potential-vorticity flow is obtained by adjusting the floor of the upstream reservoir to the desired depth. Figure 8 (*a*) shows the theoretical curves (solid line) of transport against the difference in the fluid levels between the two basins for three potential vorticities, $\lambda' = 0{\cdot}3$, $\lambda' = 0{\cdot}6$ and $\lambda' = 0{\cdot}94$, where $\lambda' = fb_m/(g'H_u)^{\frac{1}{2}}$ is the dimensionless form of the potential vorticity. The curves are obtained from (3.7) by normalizing it with respect to the critical transport at the respective potential vorticity. The similarly normalized measurements are given on the same figure as the crosses. The agreement with the theory is apparent; i.e. the transport decreases as ΔH becomes small. For

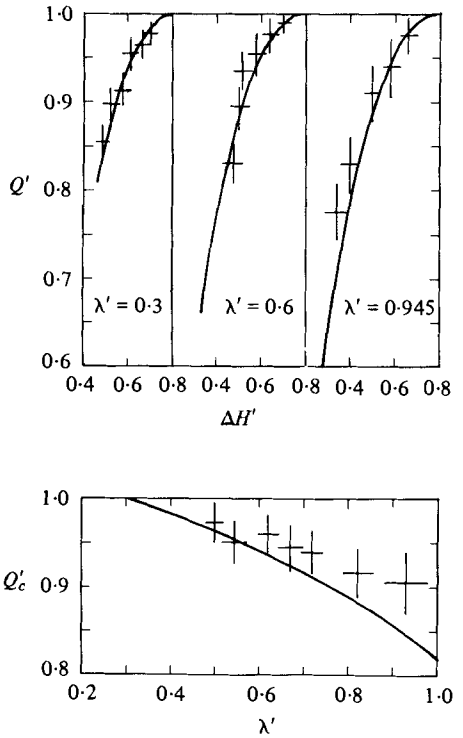

FIGURE 8. (*a*) Transport, $Q' = Q/Q_c$ versus $\Delta H' = \Delta H/h_u$ for three finite-potential-vorticity, submerged weir-flows, $\lambda' = 0{\cdot}3$, $0{\cdot}6$, and $0{\cdot}94$, where $\lambda' = fb/(g'H_u)^{\frac{1}{2}}$ and Q_c is the critical transport. The lower end of each solid (theoretical) curve terminates at the subcritical separation except for $\lambda' = 0{\cdot}94$ where the separation point is out of range. (*b*) Critical transport,

$$Q'_c = Q_c(\lambda')/Q_c \ (\lambda' = 0{\cdot}3),$$

versus potential vorticity λ', where $Q_c(\lambda' = 0{\cdot}3)$ is the critical transport at $\lambda' = 0{\cdot}3$.

comparison between different values of λ', another graph is made in which the transport of the controlled flow is plotted against λ'. The result is shown in figure 8 (*b*), where both the measured (cross) and the theoretical transport (solid curve) given by (3.7) and (3.11) have been normalized with respect to the transport at $\lambda' = 0{\cdot}3$ (the actual measured transport of $\lambda' = 0{\cdot}3$ is smaller than that of the theory by about 10 %). The trend of decreasing discharge with increasing λ' is clearly shown by the measurement, in agreement with the theory. The comparison, however, appears to be less satisfactory at high λ' where the measurements attain somewhat larger value. This larger value does not appear to be caused by friction which would likely have reduced the transport. The conjecture here is that it might be caused by upwelling in the basin, since the upwelling can conceivably affect the vorticity of the flow by vortex stretching – which is given by the upwelling rate over the depth. For a deep basin, the upwelling has no consequence, but for a shallower one the stretching effect may be magnified.

5.2. *Controlled flow through a truncated channel*

In this experiment the measurements are obtained for a zero-potential-vorticity fluid only (the actual potential vorticity is $0{\cdot}1$; as before it can be regarded as zero). As in Whitehead *et al.* (1974), the experiment is carried out by holding the transport constant

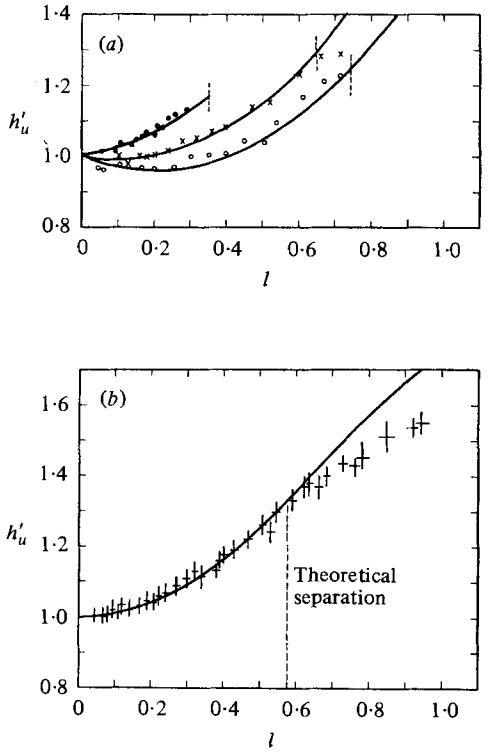

FIGURE 9. Upstream height, $h'_u = h_u/h_{u0}$, of the zero-potential-vorticity controlled flow versus rotation, $l = fb/(8g'h_{u0})^{\frac{1}{2}}$, for different cross channel bottom slopes, $\beta = sb/2h_{u0}$ where h_{u0} is the upstream height at the zero rotation and is referenced to the highest point of the floor as opposed to the average height of the floor. The dashed line on each curve indicates the point of theoretical separation. The formula for each curve is given in table 2. The experimental points are indicated (*a*) ●, $\beta = -0{\cdot}22$; ×, $\beta = 0{\cdot}40$; ○, $\beta = 0{\cdot}94$. (*b*) All points for $\beta = 0$.

Slope	Range	Formula
$\beta > 0$	$h'_u \geqslant 4l^2 - \beta$ (non-separated)	$h'_u = [(1+\beta)^{\frac{3}{2}} - (\frac{3}{4})^{\frac{1}{2}}\beta l]^{\frac{2}{3}} + l^2 - \beta$
$\beta < 0$	$h'_u \geqslant 4l^2 - 2\beta$ (non-separated)	$h'_u = [(1-\beta)^{\frac{3}{2}} + (\frac{3}{4})^{\frac{1}{2}}\beta l]^{\frac{2}{3}} + l^2 - \beta$
$\beta = 0$	$h'_u \geqslant 4l^2$ (non-separated)	$h'_u = l^2 + 1$
$\beta = 0$	$h'_u \leqslant 4l^2$ (separated)	$h'_u = 2l^2 + (\frac{2}{3})\,(l^{-1}/\sqrt{3})$

$\beta = sb/2h_{u0}$, $l = fb/(8g'h_{u0})^{\frac{1}{2}}$, $h'_u = h_u/h_{u0}$.

TABLE 2. Upstream height formulae for the curves in figure 9

and measuring the upstream height at various rotation rates. Since the transport is constant, normalizing the transport now becomes equivalent to normalizing the upstream height. The convenient reference height for normalization here is the upstream height for no rotation. The theoretical curves of the normalized upstream height h'_u against the dimensionless rotation rate l for various values of β, the dimensionless slope of the truncated floor, are shown in figure 9 (*a*) and (*b*). The formulae that

correspond to each curve are given in table 2. These formulas are obtained by normalizing (3.21) with the transport for no rotation. (Here, again, the maximum elevation of the channel floor is used as the reference level for measuring height, and so in (3.21) $\bar{\eta}$ is equal to $-\frac{1}{2}b|s|$.) Each of the curves in figure 9(*a*) and (*b*) has two regimes separated by a vertical dashed line. To the left of the line are critical flows without separation, and to the right are separated critical flows defined by $v_0 = 0$ (see § 3.2) if $\beta \geqslant 0$ and by the intersection of the free surface with the floor if $\beta < 0$. Similarly normalized measurements are also given in figure 9(*a*) and (*b*). It can be seen that in the non-separated flow regime, the agreement with theory is quite satisfactory. In the case of $\beta = 0$, the measurements follow the curve closely and show clearly that a greater hydrostatic pressure is required to drive the flow at high rotation. For $\beta > 0$ the measurements also follows the curve. In particular the interesting small drop in h'_u is clearly confirmed by the experiment. Furthermore, figure 9(*a*) shows that h'_u for $\beta > 0$ is on the average lower than that of the case for $\beta \leqslant 0$, indicating that a positive slope favours the transport. The generally good agreement with the theory just described however, fails in the separated flow regime (figure 9(*b*), shown only for the $\beta = 0$ case). The possibility of the breakdown of the theory in this regime has been noted earlier in § 3 (note that the lower measured value implies a greater transport than that of the theory; this rules out friction as a cause of the discrepancy). The theory there shows that if a separated flow is to occur, a stagnant fluid region must form to the right of this flow. It is felt that the stagnant region cannot be maintained downstream and a separated flow such as given by the theory may not be realized. The measurements apparently agree with such an assessment. In the experiment, some visual observations of the separated flow are also made. It is observed that the upstream boundary current that enters the channel becomes narrower than the channel entrance at high rotation, and there does appear to be a tendency for the stagnant region to develop near the right corner of the entrance. But, immediately after the boundary current enters the channel, the current is deflected by the rotation to the right-hand wall, causing the stagnant region to break down and the flow to become non-uniform. Figure 4 is a series of pictures of the top and side view of the channel flow, and one can see the deflection of the current from the left wall to the right wall at higher rotation rate.

In the separated regime, our measurements of h'_u are lower than those obtained in the earlier experiment by Whitehead *et al.* (1974). The cause of the discrepancy is probably the entrance geometry they used: they did not smooth the left entrance wall as is done here. Our measurements, using their geometry, also give larger values of h'_u.

5.3. *The supercritical separation*

This experiment uses a flared channel which has a rectangular cross section but the width of the channel broadens downstream. Since the controlled flow occurs in the narrowest section and the flow is subcritical upstream, the flared section downstream is therefore expected to produce the desired supercritical flow. The theory in § (3) predicts a separation of the supercritical flow from the left wall at some point downstream of the channel. In this experiment, visual evid ence is obtained of the separation and the points of separation are measured. The visual evidence is shown in figure 5, which gives both top and side view of the current. Figure 5 (photo 1) is a photo of the flow at zero rotation; the flow can be seen to broaden symmetrically as it leaves the

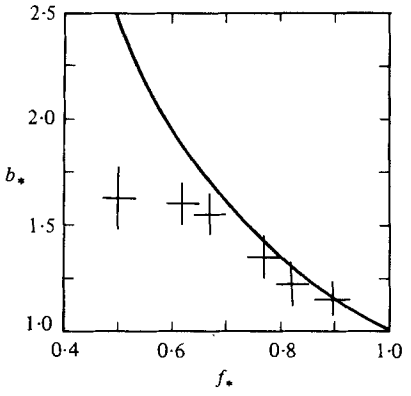

FIGURE 10. The width of the current, $b_* = b/b_m$, at the point of supercritical separation as a function of the rotation, $f_* = f/f_m$, where b_m and f_m are respectively the width and the rotation at which the supercritical separation occurs in the control section.

control section. The next few photos are taken at increasingly higher rotation rates. These photos clearly show the gradual deflection of the flow to the right and the separation of the flow from the left wall. One may also note the progressive upstream displacement of the separation point as the rotation increases, i.e. the width of the separated flow decreases as rotation increases. This width is measured in the experiment and can now be compared with the theoretical prediction of the width given by (3.23). For comparison, it is helpful to normalize the frequency of the rotation by the frequency at which the flow separates at the control section, and the width of the separation by the width of the control section. In this case, (3.23) becomes

$$b_*^4 + (2f_*^{-\frac{3}{2}} - 3f_*^{-2} - 1)\, b_*^2 + f_*^{-3} = 0,$$

with $b_* = b/b_m$ and $f_* = f/f_m$, where $f_m = (8g'Q/b_m^4)^{\frac{1}{5}}$.

The theoretical curve given by (3.23) is shown in figure 10 as a solid curve. In this figure, $f_* = 1$ and $b_* = 1$ represent the separation in the control section and for $b_* > 1$, the separation occurs in the flared section. The measurements in the same figure show an initial tendency to follow the curve starting from $f_* = 1$, but depart significantly further downstream. The discrepancy is due to the large curvature of the wall downstream which cannot be accounted for by this simple theory. In conjunction with this experiment, it will be noted that the critical transport obtained for this flared channel shows the same relation with the rotation as that shown in figure 9 (*b*). Hence the control flow is independent of the downstream geometry.

6. Conclusion and discussion

The foregoing comparisons between theory and experiment are generally favourable. The investigation has confirmed the existence of the controlled (critical) flow which has been verified in three different experiments. In particular, the controlled flow is shown in each of the three experiments to be independent of the downstream conditions, namely, the fluid level of the downstream basin and the geometry of the channel downstream of the control section. The insensitivity of the controlled flow to the downstream conditions is thus in strong support of the concept of hydraulic

control. The investigation does, however, leave open the question concerning the mechanics of the separated critical flow. Hydraulic theory is shown to be incapable of describing this flow; a more detailed theoretical and experimental investigation in the future is required. Another unsatisfactory aspect of the investigation is the effect of friction. Even though it did not seem to have affected the experimental verification, in the sense that it did not alter the predicted relationships between the measured parameters, it was believed to be the main cause of the consistent overprediction of the measured transport by theory. An understanding of the processes through which the friction modifies the transport should be helpful in improving the prediction. Finally, an aspect of the experimental design that may also need some future studies and improvements is the upwelling in the upper basin. This could not be avoided owing to the limited size of the apparatus. The upwelling is believed to have contributed to some of the discrepancies in the measurement of the high-potential-vorticity flow. In future experiments, it may be desirable to eliminate upwelling with a different experimental design. But, on the other hand, the experiment with upwelling perhaps still should be investigated since the actual ocean basin is also finite, and, moreover, the dense water in some of the ocean basins such as the Norwegian basin is believed to be formed by the sinking of surface-cooled water (Worthington 1970) which is similar to the upwelling in the experiment.

The results obtained in this paper on the submerged weir-flow, on the flow through an irregular channel, and on the supercritical separation may be added to the previous hydraulic results in their application to the study of the ocean currents in straits and sills. The present result on the flow through channels of irregular cross section should now make it possible to account for the actual geometry of the sill, especially for the zero-potential-vorticity current for which the result has been obtained. The previous applications by Stalcup *et al.* (1975), and Lonsdale (1976) are examples suitable for re-examination with our results; they studied currents in the low latitude region where the radius of deformation of the current is usually greater than the width of the sill and the flow has zero potential vorticity. In the case studied by Lonsdale (1976), the current flows into the Panama Basin, which is close to the equator and non-rotating hydraulics applies. His case can be computed quite simply with (3.19) using $f = 0$. The calculation gives about 15 % higher transport than his observed value. (The transport calculated by him assuming an equal area rectangular channel is slightly lower than that observed.) After making allowance for friction which is obviously present in his observations and, say, a correction for the friction of 10–15 % similar to that given by our experiment, the value is now approximately that which was observed. Of course, the size of the correction used here, as well as the significance of the 15 % difference may be questioned. But, the consideration of realistic geometry does appear to be consistent in view of the presence of friction. The flow studied by Stalcup *et al.* (1975) in the Anegada–Jungfern Passage of the Caribbean sea is more affected by rotation. They did not show a cross section of the control sill. But, if one assumes a parabolic shape cross section as they have shown for the section upstream of the sill, the computation should also yield a greater transport than that obtained with an equivalent area rectangular section. The only other application with the rotating weir appears to be by Whitehead *et al.* (1974). They studied the flow of Norwegian water through the Denmark Strait. This strait is in the high latitude region where the radius of deformation is more comparable to the width of the channel. Therefore, the flow is likely to

have finite potential vorticity. The present result on the irregular channel geometry has not been extended to the finite-potential-vorticity flow. But the effect of the geometry on the flow is probably qualitatively similar to that noted in § 3. Judging from the cross section of the sill given by Whitehead *et al.*, it appears that the geometry favours more transport than the one having an idealized rectangular shape since the sill is deeper on its left-hand side, i.e. the high-velocity side. Their previous estimate of the transport obtained by assuming a rectangular channel has been somewhat lower. Consideration of the real geometry can probably increase their estimate. They also noted that the current in the sill is separated. In this case the transport can be increased even more if one accepts and uses the empirical results obtained in this paper.

The other results on the submerged weir-flow and the supercritical boundary current may also have application in the ocean. So far there seems to be a lack of adequate field observation of these two types of flows. Future field measurements and comparison with the hydraulic results can be of interest.

I am indebted to Dr M. E. Stern for arousing my interest in the topic and his valuable comments on this work. I thank Dr J. C. McWilliams and Dr B. A. Taft for providing the opportunity for the preparation of the manuscript at the University of Washington, and the financial support of the National Science Foundation under grant OCE 79-0187 is acknowledged. This research was conducted at the University of Rhode Island. My gratitude is extended to Dr R. Lambert for his financial support at URI.

Appendix. Momentum and specific energy of the controlled flow

The purpose of this appendix is to define the momentum and the specific energy of the controlled flow mentioned in § 2. These two quantities have been found useful in non-rotating hydraulics for characterizing the controlled flow, in the sense that they are minimum with respect to the critical speed, as well as for studying other channel flow problems, for example, the hydraulic jumps of the supercritical flows. A definition of these two quantities for the rotating flow is, therefore, warranted. Furthermore, based on the momentum and the specific energy defined here, one can proceed in a manner as outlined by Gill (1977) and Stern (1979) to demonstrate the results given in § 2 concerning the hydraulic control. The possibility of this will be briefly indicated below.

The definition of the momentum can be obtained by integrating the shallow-water equation (2.1*a*) over the cross-section of the current, from x_1 to x_2 and from η to h. For the x-component of the equation, the integration yields a simple balance between the integrated coriolis force and the hydrostatic pressure force, which is of no interest here. For the y-component, the integrated momentum balance is

$$\frac{d}{dy}\int_{x_1}^{x_2} Hv^2 + \tfrac{1}{2}gH^2 - f\psi\, dx = -W, \tag{A 1}$$

where

$$W = -\tfrac{1}{2}g[(H^2\, dx_2/dy)_{x_2} - (H^2\, dx_1/dy)_{x_1}] - fQ\, dx_2/dy + g\int_{x_1}^{x_2} H\, \partial\eta/\partial y\, dx$$

is the sum of the pressure forces exerted by the channel on the flow. The two terms in the bracket are evaluated at x_1 and x_2 as indicated by the subscripts and are zero if the

channel has no vertical side walls. The integral on the left-hand side of (A 1) will now be defined as the momentum of the rotating open channel flow and will be denoted by

$$M = \int_{x_1}^{x_2} (Hv^2 + \tfrac{1}{2}gH^2 - f\psi)\, dx \tag{A 1a}$$

or

$$M = \int_{\psi_1}^{\psi_2} (v + gH/2v - f\psi/vH)\, d\psi. \tag{A 2b}$$

For $f = 0$, M reduces to its familiar form for the non-rotating flow. The effect of the rotation is to introduce a term $f\psi$ which represents the momentum due to the deflection of streamlines by the coriolis force.

With the definition (A 2) one can now compute the velocity at the minimum of M using the solutions (3.1) and (3.2) for the constant-potential-vorticity flow and compare it with the velocity given by (3.11). The calculation assumes constant transport, so H_0 in (3.1) and (3.2) can be replaced by v_0 and M minimized with respect to v_0. The minimum is calculated numerically, and the two velocities are indeed the same. A comparison is also made with the speed computed from the critical flow formula given by Stern (1974). The same result is again obtained. Hence the minimum momentum represents the controlled flow.

A definition of the specific energy consistent with that given in nonrotating hydraulics can be obtained by integrating (2.2) over the cross section of the current and making use of (2.4). The result of the integration is simply $dE_0/dy = 0$, where E_0 is given by (2.7). The specific energy can now be defined as $E_t = E_0 - \eta_0$ which is essentially the Bernoulli energy measured relative to the channel floor. Thus the equation for the specific energy is just

$$dE_t/dy = -d\eta_0/dy, \tag{A 3}$$

since E_0 is constant. It should be noted that E_t along $x_2 = 0$ is used strictly for convenience: its value along other streamlines can also be used.

With the above definition for E_t, it is easily seen that minimizing E_t is basically the same as minimizing η_0. Hence, for the constant-potential-vorticity flow, the critical speed computed with (3.11) is also the one that gives the minimum specific energy.

The statements about the minimum of the momentum and the specific energy are shown above to be applicable to the controlled, constant-potential-vorticity flow. In order to show their applicability to controlled rotating flow in general, the procedure outlined by Gill (1977) or the 'control' rule given by Stern (1979) can be invoked. As an illustration, consider the simple example of the flow in a channel of variable elevation but of constant width. For the flow in this channel, the flow variables are functions of two parameters only, and let these be Q and v_0 which follow from (2.5), (2.6) and (2.8). Thus, for a constant transport, (A 1) and (A 3) are respectively,

$$(\partial M/\partial v_0)(dv_0/dy) = -\int_{x_1}^{x_2} gH\, \partial\eta/\partial y\, dx \quad \text{and} \quad (\partial E_t/\partial v_0)(dv_0/dy) = -g\, \partial\eta_0/\partial y.$$

These two relations show that at $\partial\eta/\partial y = 0$, $\partial M/\partial v_0$ and $\partial E_t/\partial v_0$ must also vanish. Differentiating the above relations once more with respect to y at $\partial\eta/\partial y = 0$, one has

$$(\partial^2 M/\partial v_0^2)(dv_0/dy)^2 = -\int_{x_2}^{x_1} gH\, \partial^2\eta/\partial y^2\, dx,$$

and

$$(\partial^2 E_t/\partial v_0^2)\,(dv_0/dy)^2 = -gd^2\eta_0/dy^2.$$

Thus, at the constriction, i.e. at the maximum elevation η, both M and E_t are minimized with respect to the velocity v_0. One constraint which the above imposes is that $dv_0/dy \neq 0$. As a result, the speed must change continuously across the constriction, for example from subcritical to supercritical, or vice versa. The constriction, at which the least momentum and the specific energy are achieved, is also a constriction with respect to the width, even though the foregoing has considered only the constriction with respect to the elevation. This follows from (A 1) which shows that at the section of the smallest M, a downstream decrease in the width will further decrease M. Since a steady solution cannot be realized for M less than its smallest value, the width therefore must be the narrowest at the constriction.

Two remaining results in § 2 can also be shown here, namely, that the controlled flow also has the maximum transport at either a constant M or a constant E_t and that the critical speed equals the long-wave speed. For the first one, assume that $M(Q, v_0)$ = constant. Then $\partial M/\partial v_0 + (\partial M/\partial Q)\,(dQ/dv_0) = 0$ which shows that at the critical speed $dQ/dv_0 = 0$ since $\partial M/\partial v_0 = 0$. The second derivative of M at $\partial M/\partial v_0 = 0$ is $\partial^2 M/\partial v_0^2 + (\partial M/\partial Q)\,(d^2Q/dv_0^2) = 0$. Therefore, the transport is a maximum since $\partial^2 M/\partial v_0^2 > 0$ and $\partial M/\partial Q > 0$. The fact that $\partial M/\partial Q > 0$ can be seen from (A 2) where H increases with Q at fixed v_0, and hence M is proportional to Q. For the second result, assume a uniform channel for which W in (A 1) is zero. For a flow with a stationary disturbance, (A 1) is simply $dM/dy = 0$ or $(\partial M/\partial v_0)\,(dv_0/dy) = 0$, where v_0 contains both a mean current and a small disturbance. Since for the perturbation dv_0/dy is non-zero, $\partial M/\partial v_0$ must vanish. For an infinitesimal disturbance, this implies that the velocity, which gives the minimum momentum, is also the long-wave speed.

REFERENCES

Chow, V. T. 1959 *Open-Channel Hydraulics*. McGraw-Hill.

Gill, A. E. 1976 Adjustment under gravity in a rotating channel. *J. Fluid Mech.* **77**, 603.

Gill, A. E. 1977 The hydraulics of rotating channel flow. *J. Fluid Mech.* **80**, 641.

Houton, R. E. 1907 Weit Experiments: Coefficients and formulas. Dept. of Interior U.S. Geological Survey, Government Printing Office, Washington, D.C.

Lonsdale, P. 1977 Inflow of bottom water to the Panama Basin. *Deep-Sea Res.* **24**, 1065.

Rouse, H. 1961 *Fluid Mechanics for Hydraulic Engineers*. Dover.

Sambuco, E. & Whitehead, J. 1976 Hydraulic control by a wide weir in a rotating fluid. *J. Fluid Mech.* **73**, 521.

Stalcup, M. C., Metcalf, W. G. & Johnson, R. G. 1975 Deep Caribbean inflow through the Anegada-Jungfern passage. *J. Marine Res.* **33**, 15.

Stern, M. E. 1974 Comment of rotating hydraulics. *Geophys. Fluid Dyn.* **6**, 127.

Stern, M. E. 1972 Hydraulically critical rotating flow. *Phys. Fluids* **15**, 2062.

Stern, M. E. 1980 A variational principle for turbulent flow. *Phys. Fluids* **23**, 2161.

Whitehead, J., Leetmaa, A. & Knox, R. A. 1974 Rotating hydraulics of strait and sill flows. *Geophys. Fluid Dyn.* **6**, 101.

Worthington, L. V. 1970 The Norwegian Sea as a mediterranean basin. *Deep-Sea Res.* **17**, 77.